Supporting Information

Biocontrol application and the delay-differential equations

Since we were also initially interested in analyzing how the timing of control strategies within a season influences long-term population dynamics, we used a modified version of the delay differential equations (eqs. 1-2). These modified equations preserve the delay between infection and pathogen release throughout the season and give us the ability to add either Gypchek or Bt to the system at any time after larvae emerge from the egg masses.

Our within-season model can be divided into two parts: 1) an initial period of length $\widehat{t}$ in which neonate larvae are infected as they emerge from their egg masses with virus Z_T surviving from the previous season, and 2) a much longer period $\widehat{t}$ to pupation at time t_F during which larvae are infected by ingesting virus $P(t)$ produced in the current season (or applied as biocontrol). This period from $\widehat{t}$ to t_F is further subdivided into three parts to explicitly incorporate the delay of length τ between infection (by either P or Z) and pathogen release. In total, the full within-season model consists of four separate sets of equations outlined below:

1) Period $0 < t < \widehat{t}$ during which the neonate larvae, which are more susceptible than the older instars, emerge from their egg masses and are exposed to overwintering pathogen contaminating the eggs or nearby bark (Murray & Elkinton 1989, 1990). Given the increased susceptibility, the transmission rate $\bar{\nu}$ is scaled by a factor, ρ. No biocontrol is permitted during this window as the larvae have not yet begun to feed on foliage and no natural pathogen has yet been produced. Thus, there is only a decline in the number of

susceptibles.

$$\frac{dS}{dt} = -\rho\overline{\nu}\left[\frac{S(t)}{S(0)}\right]^{V} Z(t)S(t) \tag{S1}$$

$$\frac{dP}{dt} = 0 \tag{S2}$$

2) Period $\widehat{t} < t < \tau$, when larvae have reached the foliage and no longer contact pathogen Z. No natural pathogen has yet been produced. Pathogen in the system would only be due to the addition of Gypchek.

$$\frac{dS}{dt} = -\overline{\nu}\left[\frac{S(t)}{S(0)}\right]^{V} P(t)S(t) \tag{S3}$$

$$\frac{dP}{dt} = 0 \tag{S4}$$

3) Period $\tau < t < \tau + \widehat{t}$ during which neonate larvae naturally infected by the overwintering pathogen Z die and release the first round of natural pathogen. Susceptibles decline as they begin to encounter this new pathogen.

$$\frac{dS}{dt} = -\overline{\nu}\left[\frac{S(t)}{S(0)}\right]^{V} P(t)S(t) \tag{S5}$$

$$\frac{dP}{dt} = \rho\overline{\nu}\left[\frac{S(t-\tau)}{S(0)}\right]^{V} Z(t-\tau)S(t-\tau) \tag{S6}$$

4) Period $\tau + \widehat{t} < t < t_F$, which represents upwards of 75 percent of the season, when larvae are infected with pathogen produced earlier in the same season and die, producing more pathogen P. Multiple rounds of transmission are possible. Pathogen decay is included during this period but not earlier to maintain similarity with Dwyer *et al.* (2000). Including

pathogen decay rate μ in the earlier equations has very little impact on model behavior.

$$\frac{dS}{dt} = -\overline{\nu}\left[\frac{S(t)}{S(0)}\right]^V P(t)S(t) \tag{S7}$$

$$\frac{dP}{dt} = \overline{\nu}\left[\frac{S(t-\tau)}{S(0)}\right]^V P(t-\tau)S(t-\tau) - \mu P(t) \tag{S8}$$

Rescaling

To better understand the dynamics, we rescaled both the within-in (eqs. S1 - S8) and between-season (eqs. 4 - 6 in the main text) equations. The rescaled within-season equations take the form:

for $0 < t < \widehat{t}$

$$\frac{d\widetilde{S}}{dt} = -\mu\left[\frac{\widetilde{S}(t)}{\widetilde{S}(0)}\right]^V \widetilde{Z}\widetilde{S}, \tag{S9}$$

$$\frac{d\widetilde{P}}{dt} = 0, \tag{S10}$$

for $\widehat{t} < t < \tau$

$$\frac{d\widetilde{S}}{dt} = -\mu\left[\frac{\widetilde{S}(t)}{\widetilde{S}(0)}\right]^V \widetilde{P}\widetilde{S}, \tag{S11}$$

$$\frac{d\widetilde{P}}{dt} = 0, \tag{S12}$$

for $\tau < t < \tau + \widehat{t}$

$$\frac{d\widetilde{S}}{dt} = -\mu \left[\frac{\widetilde{S}(t)}{\widetilde{S}(0)}\right]^V \widetilde{P}\widetilde{S}, \tag{S13}$$

$$\frac{d\widetilde{P}}{dt} = \mu \left[\frac{\widetilde{S}(t-\tau)}{\widetilde{S}(0)}\right]^V \widetilde{Z}(t-\tau)\widetilde{S}(t-\tau), \tag{S14}$$

for $\tau + \widehat{t} < t < t_F$

$$\frac{d\widetilde{S}}{dt} = -\mu \left[\frac{\widetilde{S}(t)}{\widetilde{S}(0)}\right]^V \widetilde{P}\widetilde{S}, \tag{S15}$$

$$\frac{d\widetilde{P}}{dt} = \mu \left[\frac{\widetilde{S}(t-\tau)}{\widetilde{S}(0)}\right]^V \widetilde{P}(t-\tau)\widetilde{S}(t-\tau) - \mu\widetilde{P}. \tag{S16}$$

Rescaled between-season equations are:

$$\widetilde{N}_{T+1} = \lambda\widetilde{N}_T(1-I_T)\left[1 - \frac{2a\widetilde{b}\widetilde{N}_T}{\widetilde{b}^2 + \widetilde{N}_T^2}\right] \tag{S17}$$

$$\widetilde{Z}_{T+1} = \phi\widetilde{N}_T I_T + \xi\widetilde{Z}_T \tag{S18}$$

$$I_T = 1 - \left[\frac{\widetilde{S}(t_F)}{\widetilde{S}(0)}\right] \tag{S19}$$

Definitions of rescaled within-season variables are:

$$\widetilde{S}(t) \equiv \frac{\overline{\nu}}{\mu}S(t), \widetilde{P}(t) \equiv \frac{\overline{\nu}}{\mu}P(t), \widetilde{Z}(t) \equiv \frac{\rho\overline{\nu}}{\mu}Z(t). \tag{S20}$$

Definitions of rescaled between-season variables are:

$$\widetilde{N}_T \equiv \frac{\overline{\nu}}{\mu} N_T, \widetilde{Z}_T \equiv \frac{\rho\overline{\nu}}{\mu} Z_T, \widetilde{b} \equiv \frac{\overline{\nu}}{\mu} b, \phi \equiv \frac{\gamma}{\rho}\,. \tag{S21}$$

Note that due to rescaling, Z and P cannot be interpreted in exactly the same way. In the rescaled model above, overwintering pathogen Z can be thought of as more infective due to the lower doses needed to infect neonate larvae when $t < \widehat{t}$. There is no new pathogen P during this interval.

Since the timing of the biocontrol addition during the within-season period did not affect overall dynamics for computational efficiency, we used the rescaled versions of the discrete difference equations throughout our analyses (eqs. 4-6) where:

$$\widetilde{N}_{T+1} = \lambda \widetilde{N}_T (1 - I_T) \left[1 - \frac{2a\widetilde{b}\widetilde{N}_T}{\widetilde{b}^2 + \widetilde{N}_T^2} \right] \tag{S22}$$

$$\widetilde{Z}_{T+1} = \phi \widetilde{N}_T I_T + \xi \widetilde{Z}_T \tag{S23}$$

$$I_T = 1 - \left\{ 1 + V[\widetilde{N}_T I_T + \widetilde{Z}_T] \right\}^{-1/V}. \tag{S24}$$

We substituted the non-dimensionalized host and pathogen densities where $\widetilde{N}_T \equiv \frac{\bar{\nu}}{\mu} N_T$ and $\widetilde{Z}_T \equiv \frac{\bar{\nu}\eta}{\mu} Z_T$. $\widetilde{b}$ is defined as $\frac{\bar{\nu}}{\mu} b$ and $\phi \equiv \gamma\eta$.

Using either the delay-differential equations or the discrete difference equations, the addition of biocontrol takes one of two forms. Either it increases the pathogen by P_G if Gypchek is applied or it decreases the number of susceptibles by a fraction f_B if Bt is

applied. Whether or not biocontrol is applied depends upon the threshold population size N_H of an increasing population.

Sensitivity analysis

To explore how changes in model parameter values affect metrics of long-term gypsy moth population dynamics, we conducted a sensitivity analysis where we allowed host fecundity λ, the coefficient of variation associated with transmission $V^{1/2}$, overwintering survival of the pathogen ϕ, and the fraction of the pathogen that survives from the previous generation ξ to vary. Each of the parameters varied directly affects the host-pathogen interaction. The range of values used spans previously reported estimates of each parameter (Dwyer *et al.* 2000; Dwyer, Dushoff & Yee 2004). The upper bound of the coefficient of variation was set to one since values greater than one result in a stable population (Dwyer *et al.* 2000). The lower bounds were determined by model stability. For some of the parameter combinations, a value of less than 0.80 resulted in either the host or the pathogen going extinct. For our analysis, we used a non-stochastic version of the basic model (eqs. 4-6).

Regardless of the combination of parameter values, except for the extreme values of ϕ and ξ, there are relatively large portions of parameter space that exhibit similar mean cycle periods (8.1–10.5; Dwyer, Dushoff & Yee 2004) and magnitudes of population change (4–6; Dwyer *et al.* 2000; Dwyer, Dushoff & Yee 2004) as natural gypsy moth populations (Fig. S1-S2). At the largest values of ϕ and ξ, cycle periods and the magnitude of these cycles were much lower than natural dynamics indicating that the host-pathogen interaction was best characterized by a steady state. With $\xi = 0$ and as ϕ was raised, a increasing portion of the parameter space showed areas where either the host or the

pathogen went extinct. In general, the model appears relatively robust to changes in parameter values associated with the host-pathogen interaction.

Stability analysis

If we allow for a constant application of the biocontrol agent, we can perform a standard stability analysis for the system of host-pathogen equations. Stability analyses generally take the form of calculating the equilibrium points in the system and solving the Jacobian matrix at those equilibrium points (May 1974). First we consider a system where no biocontrol agents are added and then show how the equilibrium values, Jacobian matrix, and the system's stability change as the result of constant biocontrol applications.

We begin with the rescaled equations (eqs. S22-S24). For convenience, we eliminate the tilde associated with the equations and confine our analysis to nontrivial equilibriums such that both the host and the pathogen are maintained in the system. First, we assume that the system is close to its equilibrium values or in quasi-equilibrium. The pathogen density immediately adjusts to equilibrium such that $\bar{Z} = \phi\bar{N}\bar{I}/(1-\xi)$. We can then calculate the equilibrium values for the system using eq. S22. Equilibrium occurs where the functions $g(\bar{N},\bar{I}) = \lambda(1-\bar{I}(\bar{N}))$ and $h(\bar{N},\bar{I}) = 1/[1-(2ab\bar{N})/(b^2+\bar{N}^2)]$ intersect.

The Jacobian for the host-pathogen system without biocontrol addition becomes:

$$\mathbf{J} = \begin{pmatrix} \lambda\left\{(1-\bar{I})\left[1-\frac{2ab\bar{N}}{b^2+\bar{N}^2}\right] - \bar{N}I_N\left[1-\frac{2ab\bar{N}}{b^2+\bar{N}^2}\right] - \bar{N}(1-\bar{I})\left[\frac{2ab(b^2-\bar{N}^2)}{b^2+\bar{N}^2}\right]\right\} & -\lambda\bar{N}I_Z\left[1-\frac{2ab\bar{N}}{b^2+\bar{N}^2}\right] \\ \phi\bar{I}+\phi\bar{N}I_N & \phi\bar{N}I_Z+\xi \end{pmatrix},$$

where I_N and I_Z are the partial derivatives of eq. S24. I_Z equals:

$$\frac{[1+V(\bar{N}\bar{I}+\bar{Z})]^{(-1/V-1)}}{1-\bar{N}[1+V(\bar{N}\bar{I}+\bar{Z})]^{(-1/V-1)}}$$

and I_N equals $\bar{I}I_Z$. The Jacobian is then solved at the calculated equilibrium points using the parameters values from the main text. When the Jacobian is solved, there are three equilibrium points that correspond to the source, sink, and saddle-point equilibria in Figs. 2-3.

Gypchek addition

The addition of Gypchek simply adds a constant dose of pathogen to the system. This changes the equilibrium value for the pathogen such that $\bar{Z} = (\phi\bar{N}\bar{I} + P_G)/(1-\xi)$. However, it does not affect the Jacobian. Regardless of the amount of Gypchek that was sprayed, the system maintained all three equilibria (Fig. S3A). Low levels of Gypchek addition forced the system to remain in the domain of attraction near the high-density unstable equilibrium. As Gypchek additions increase, population dynamics depend upon initial conditions and in a stochastic system would most likely bounce around between attractors (Dwyer, Dushoff & Yee 2004). At higher levels of Gypchek, the second and third equilibria become stable (Fig. S3A). However, these higher levels of Gypchek never allow the population to be maintained near the equilibria. Given these results, it would appear that the change in population dynamics due to Gypchek addition depends upon the whether the addition of the pathogen forces the system into the domain of attraction for the low-density or high-density equilibrium.

Bt addition

The addition of Bt to the system changes both the equilibrium values and the Jacobian. In terms of the equilibrium values, $g(\bar{N}, \bar{I})$ is multiplied by $1 - f_B$. The same is true for the top row of the Jacobian. Not only do these changes affect the magnitude of the greatest eigenvalue but also affect the number of equilibria in the system (Fig. S3B). If the fraction killed is less than 0.70, three equilibria exist with similar magnitudes as in the original model without spraying. Above this threshold values, only the first equilibria exists, which is always stable. As is true with adding Gypchek to the system, the system exhibits a variety of behaviors dependent upon which domain of attraction it remains in.

Chaotic dynamics

To explore whether or not application of the biocontrol agent can drive the population in and out of chaos, we calculated the Global Lyapunov exponent (GLE) (Abbott & Dwyer 2007; Dennis *et al.* 2001) associated with the model. The GLE measures the degree to which separate trajectories of the same system either converge or diverge. Divergent trajectories are an indication of chaotic dynamics and correspond to a positive GLE. Convergent trajectories result in a negative GLE and indicate non-chaotic dynamics. We calculated stochastic GLEs for a variety of levels of system-wide stochasticity, trigger thresholds for spraying the biocontrol agent, and the amount of agent to be sprayed using methods outlined in Dennis *et al.* (2001). For each combination of parameters, we ran the simulation for 100,000 iterations discarding the first 1,000 to eliminate transient dynamics due to initial conditions. The GLEs are calculated using the remaining iterations.

In a stochastic environment without biological control, the long-term dynamics can be best described as chaotic (Dwyer, Dushoff & Yee 2004). The degree to which the addition of biocontrol results in chaotic or non-chaotic dynamics depends upon two factors – the threshold population size and the level of environmental stochasticity (Fig. S9). At low levels of stochasticity, the system is maintained at a single stable point or exhibits small-amplitude cycles. As stochasticity increases, the behavior of the system depends upon the threshold population size. With a constant addition of control agent or a relatively low threshold population size, relatively small additions of Gypchek result in non-chaotic dynamics. At higher additions of Gypchek, the dynamics almost always become chaotic. Adding Bt to the system while also suppressing population size almost always results in chaotic dynamics (Fig. S9). At higher Bt mortality rates with stochasticity, application of biocontrol with a low host threshold suppresses the population as it chaotically travels around a single point. Applications with a high threshold population size have little impact on the system. In general, the addition of either biocontrol agent can drive the population to either the high- or low-density equilibrium. However, the biocontrol agent determines whether the population exhibits chaotic or non-chaotic dynamics. Thus, their long-term dynamics are qualitatively quite different.

Behavior of the delay-differential equations model

The most conspicuous feature of our deterministic model is a chaotic strange attractor in the form of a large amplitude stable cycle with a variable period of approximately a decade (Fig. S10), which is similar in shape and form to the dynamics of the between-season model using the burnout-approximation (Dwyer, Dushoff & Yee 2004). This attractor is

locally stable in that trajectories originating near the attractor return to it. Inside the attractor are two equilibrium points, one a stable spiral and the other an unstable spiral. The stable point occurs at low host density, maintained by the action of the type III functional response of the generalist predators. In this scenario, the host population remains so low that the disease has little effect on dynamics. Because this point is only locally stable, if the population trajectory is perturbed enough it can escape the influence of the stable point and return to the cycle. The likelihood that this occurs is enhanced by the spiral nature of the equilibrium, which causes trajectories to dampen fairly slowly.

The unstable spiral occurs at much higher host density, and is not reachable under ordinary conditions. A saddle point exists between the two equilibria. Trajectories leaving the influence of the unstable spiral generally make two "saddle flybys" on their way to the strange attractor, but never approach the stable equilibrium. A homoclinic orbit separates the basin of attraction of the stable equilibrium from the basin of attraction of the strange attractor. There is also an unstable limit cycle separating the strange attractor from the basin of attraction of the trivial extinction equilibrium where the pathogen and host no longer exist. Trajectories forced into the basin of the extinction equilibrium reach it very rapidly, usually within a single cycle. In general, the delay differential model behaves in a similar fashion as the discrete model proposed by Dwyer, Dushoff & Yee (2004) as would be expected.

Parameter values for delay-differential equations

Table S1: Parameter values used in the simulations for the rescaled delay-differential equations, eqs. S9-S19.

parameter	value	description
τ	12	delay between infection and pathogen release in days
$\widehat{t}$	5	length of the egg mass infection period in days
t_F	69.8	length of the entire season in days
μ	0.15	within-season pathogen decay parameter
V	0.917	squared coefficient of variation of susceptibility
λ	20	host reproduction parameter
ϕ	15	between-season pathogen carryover parameter
a	0.87	maximum predation fraction
$\widetilde{b}$	0.2	host density $\widetilde{N}$ at which predation fraction $= a$
$\widetilde{N}_0$	0.3	initial condition for host density $\widetilde{N}$ at $T = 0$
$\widetilde{Z}_0$	10	initial condition for pathogen density $\widetilde{Z}$ at $T = 0$

Supporting Figures

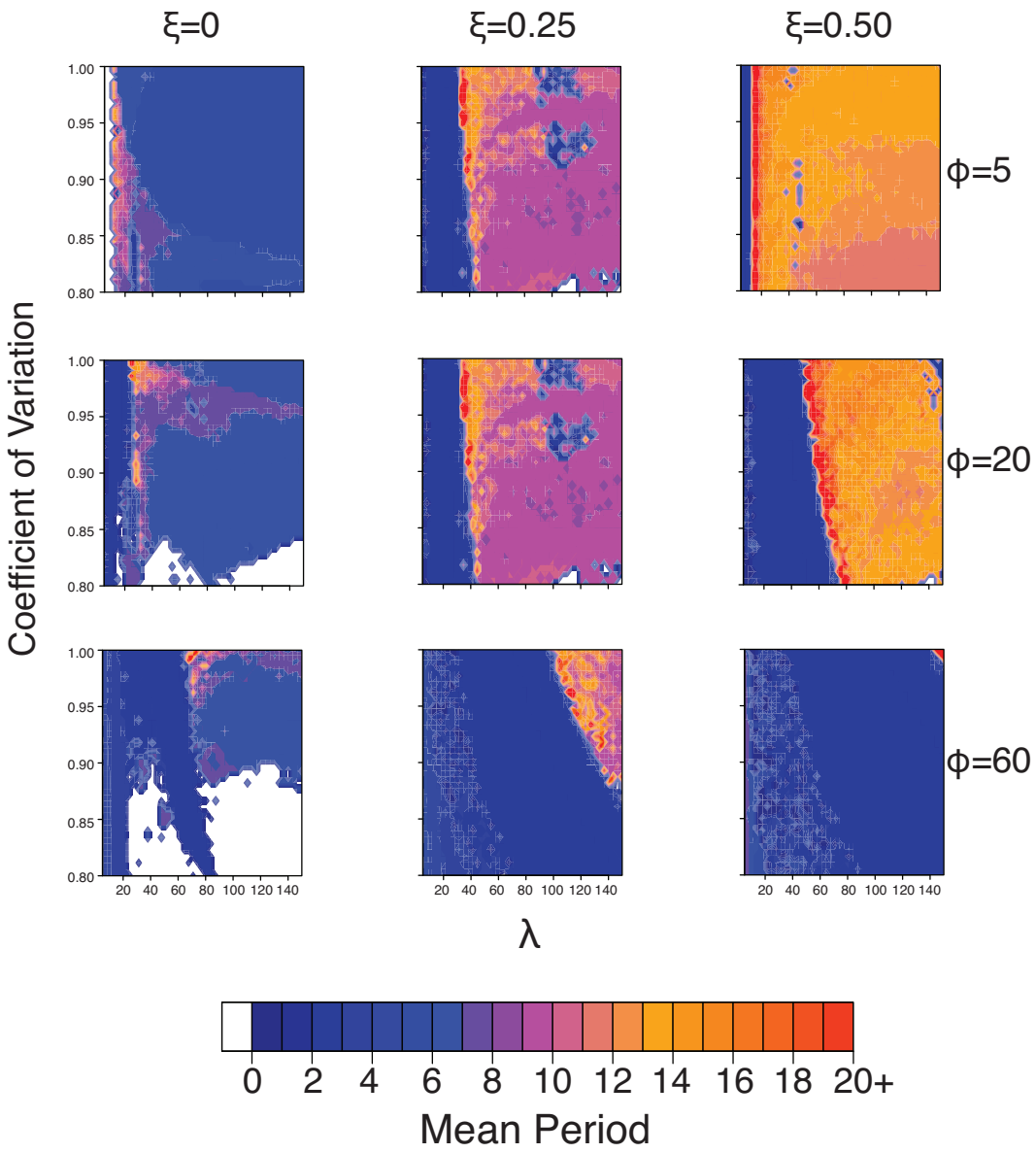

Figure S1: Effects of changes in fecundity λ, coefficient of variation $V^{1/2}$, overwintering viability of cadavers produced in the current generation ϕ and the viability of pathogen produced in previous generations ξ on the mean period between cycles. Natural populations of gypsy moths usually exhibit a mean period of 8.1 to 10.5 years (Dwyer, Dushoff & Yee 2004).

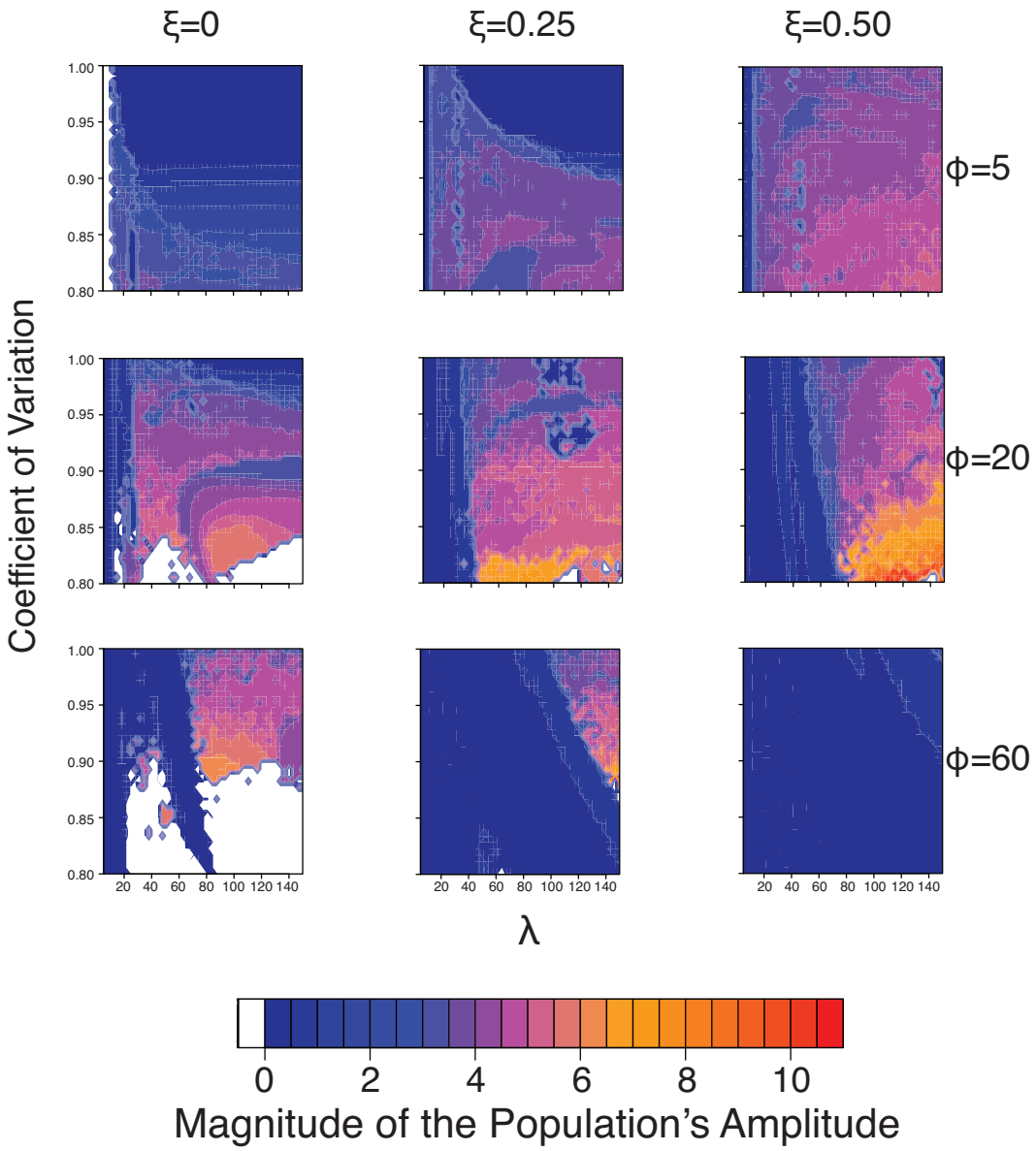

Figure S2: Effects of changes in fecundity λ, coefficient of variation $V^{1/2}$, overwintering viability of cadavers produced in the current generation ϕ and the viability of pathogen produced in previous generations ξ on the magnitude of the changes in population size from the trough to the peak of single cycle. Natural populations of gypsy moths usually exhibit changes in magnitude on the order of 4 to 6 (Dwyer, Dushoff & Yee 2004).

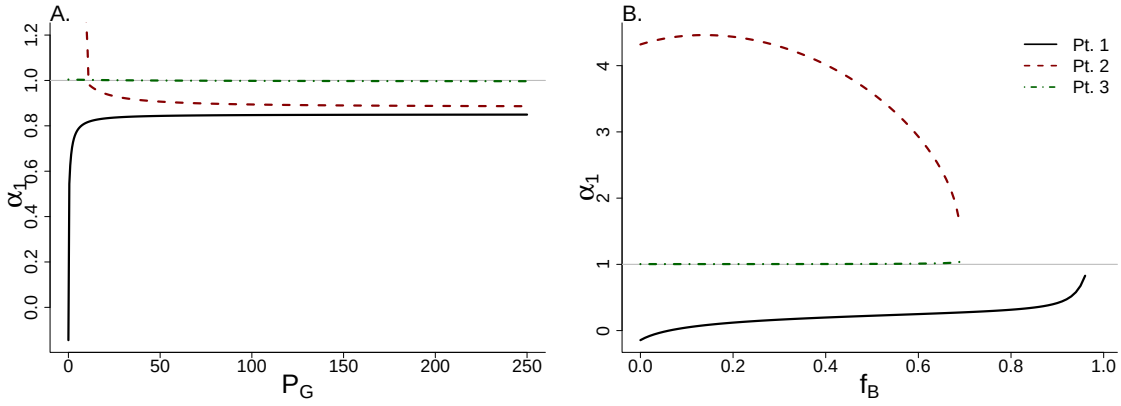

Figure S3: Effects of constant addition of either Gypchek (A) or Bt (B) on the greatest eigenvalue, α_1, as the amount of pathogen, P_G, or fraction of individuals killed, f_B, increases. Pt. 1, Pt. 2, and Pt. 3 in the legend refer to the sink, saddle-point, and source equilibria in Figs. 2-3, whose initial values are derived from the base model with no biocontrol addition. For Gypchek, the number of equilibria remains at three throughout. For Bt, as the fraction killed increases, the number of equilibrium points decreases to one. If a particular line ends before $f_B = 1$ in subfigure B, the system has dropped that equilibrium point. Note that the y-axis for A has a maximum that is less than the value for the saddle-point when small amounts of the pathogen are applied. The axis has been shrunk to improve comparison between equilibria.

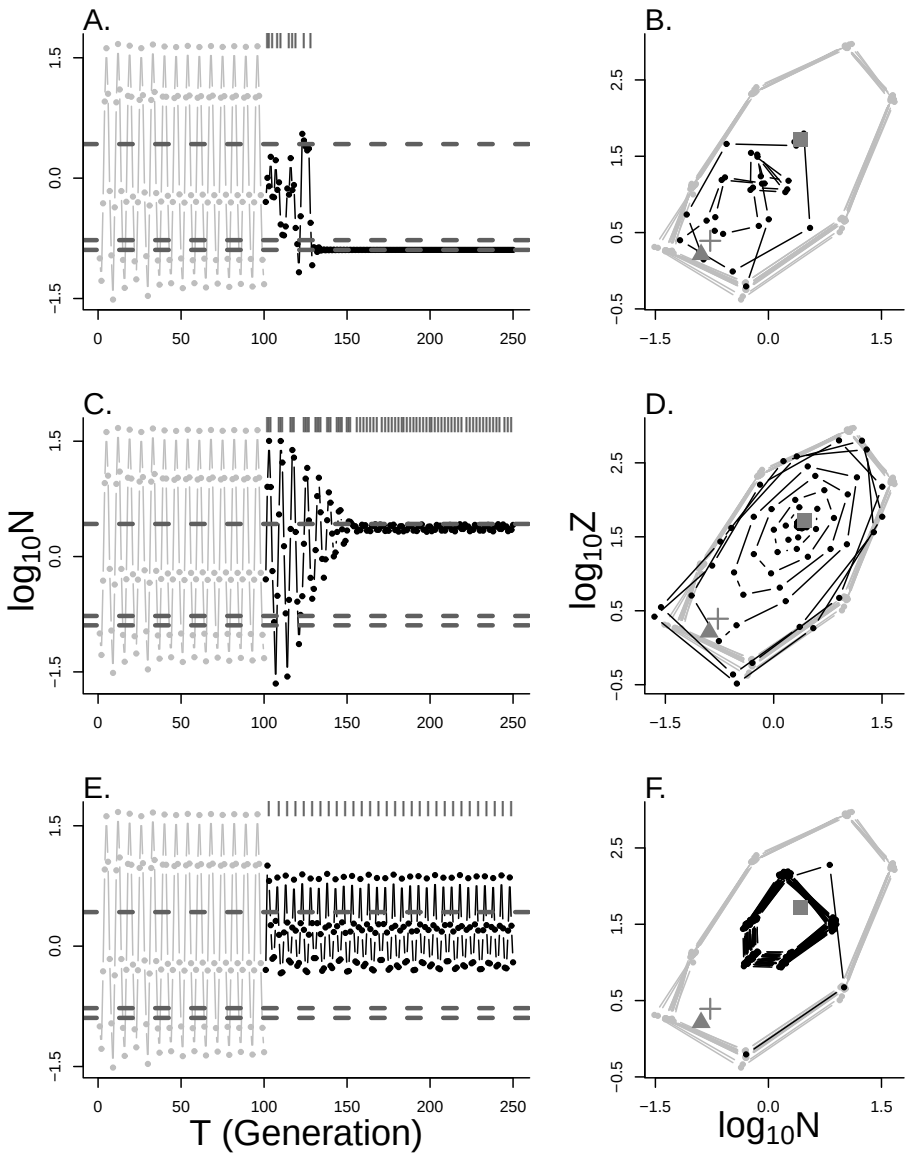

Figure S4: Time series, in the left column, and phase portraits, in the right column, of the deterministic model. Trajectories of the host population are plotted before (gray) and after (black) the beginning of the spray program at year 100. Dark gray tick marks indicate years in which Bt was applied. The dashed lines in the time series indicate the three analytical equilibria for the gypsy moth model without biocontrol addition. In the phase portraits, these equilibria are marked by the dark gray symbols that represent the source (square), sink (triangle), and saddle-point (cross) equilibria. For A and B where $f_B = 0.90$, $N_H = 0.45$, the host population is quickly sent to low-level steady state without need for continued spray treatments. For C and D where $f_B = 0.20$, $N_H = 0.25$, Bt application holds the host at a high-level steady state which would be unstable without continued application. For E and F where $f_B = 0.85$, $N_H = 3.00$, the host displays large amplitude cycles around the source.

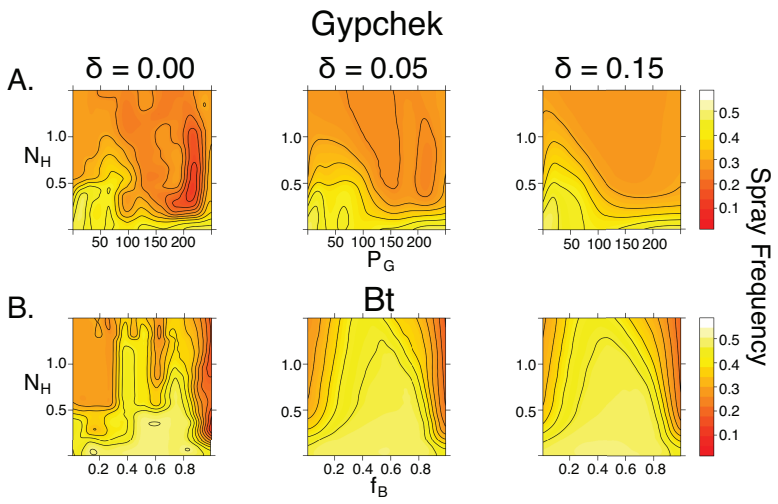

Figure S5: Summary plots of the stochastic model for a range of Gypchek, P_G, (row A) and Bt, f_B, (row B) addition versus threshold spray values, N_H, on biocontrol spray frequency. Stochasticity increases from $\sigma = 0$ in the left column to $\sigma = 0.15$ in the right column. Contour lines and shading correspond to varying levels of frequency at which the biocontrol agent was added to the system. All plots include only the 150 years following the start of the spray program. Darker/redder colors indicate relatively low frequencies of spraying.

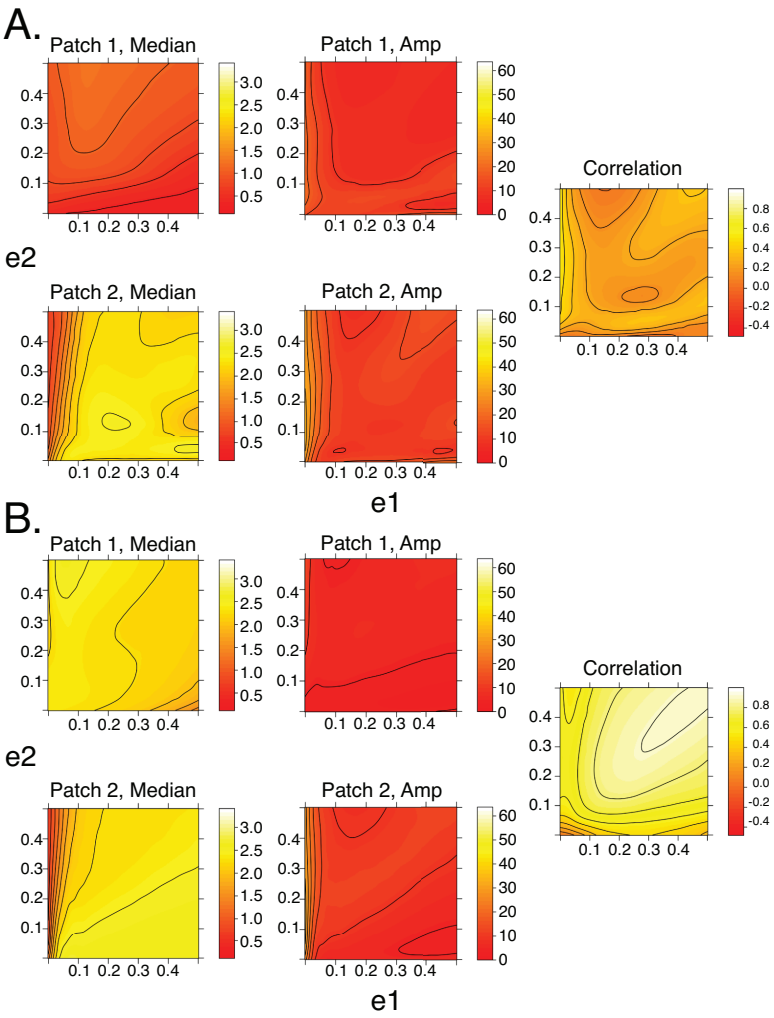

Figure S6: Effects of emigration rate between a Gypchek sprayed (Patch 1) and unsprayed (Patch 2) patch on median population size for each patch, amplitude of population swings for each patch, and the correlation between patches. Correlation between patches was measured by examining the correlation in log 10 differences in population size from one time period to the next. A) $P_G = 150$ and $N_H = 0.30$ as in Fig. 2A. B) $P_G = 10$ and $N_H = 0.15$ as in Fig. 2C. $\sigma = 0.15$ throughout each individual run. A total of 100 runs were used for each emigration parameter combination.

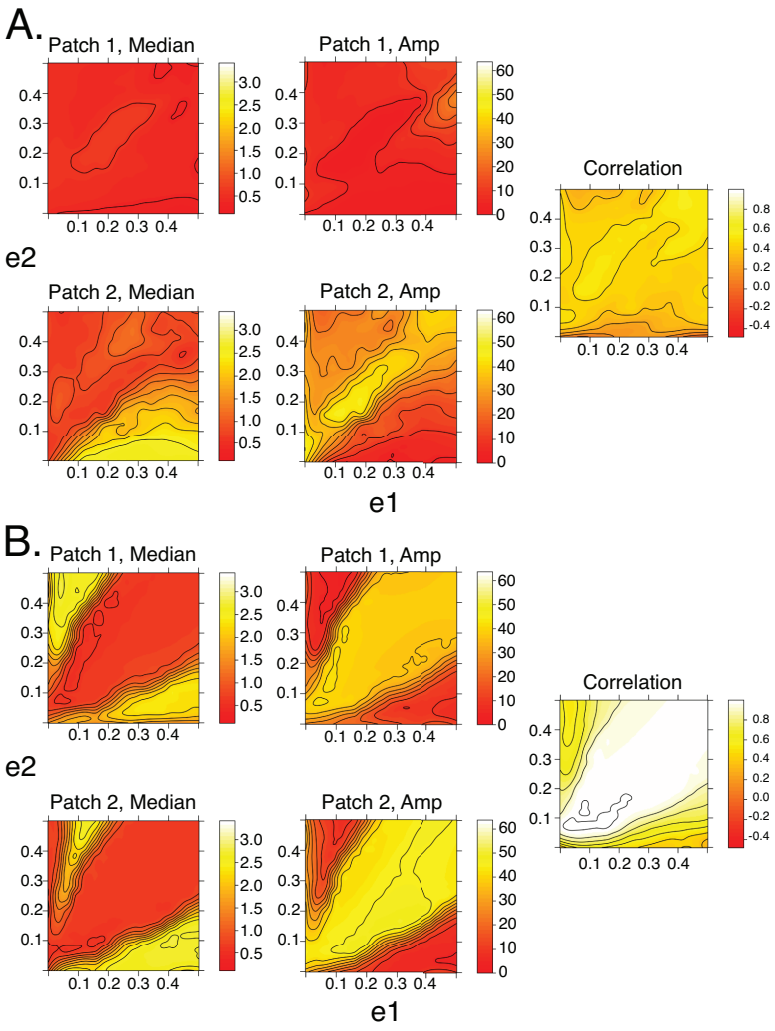

Figure S7: Effects of emigration rate between a Bt sprayed (Patch 1) and unsprayed (Patch 2) patch on median population size for each patch, amplitude of population swings for each patch, and the correlation between patches. Correlation between patches was measured by examining the correlation in log 10 differences in population size from one time period to the next. A) $f_B = 0.94$ and $N_H = 0.45$, which correspond to a low-level equilibrium in the sprayed patch, and B) $f_B = 0.15$ and $N_H = 0.45$, which correspond to a high-level equilibrium in the sprayed patch. All model runs were deterministic.

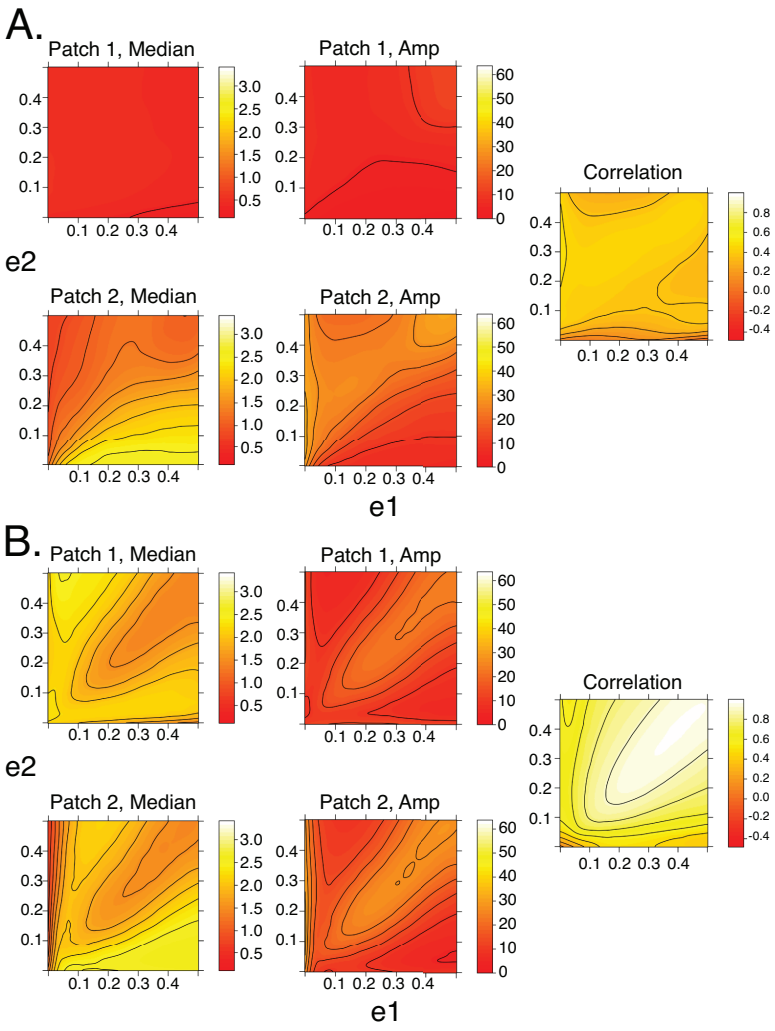

Figure S8: Effects of emigration rate between a Bt sprayed (Patch 1) and unsprayed (Patch 2) patch on median population size for each patch, amplitude of population swings for each patch, and the correlation between patches. Correlation between patches was measured by examining the correlation in log 10 differences in population size from one time period to the next. A) $f_B = 0.94$ and $N_H = 0.45$, which correspond to a low-level equilibrium in the sprayed patch, and B) $f_B = 0.15$ and $N_H = 0.45$, which correspond to a high-level equilibrium in the sprayed patch. $\sigma = 0.15$ throughout each individual run. A total of 100 runs were used for each emigration parameter combination.

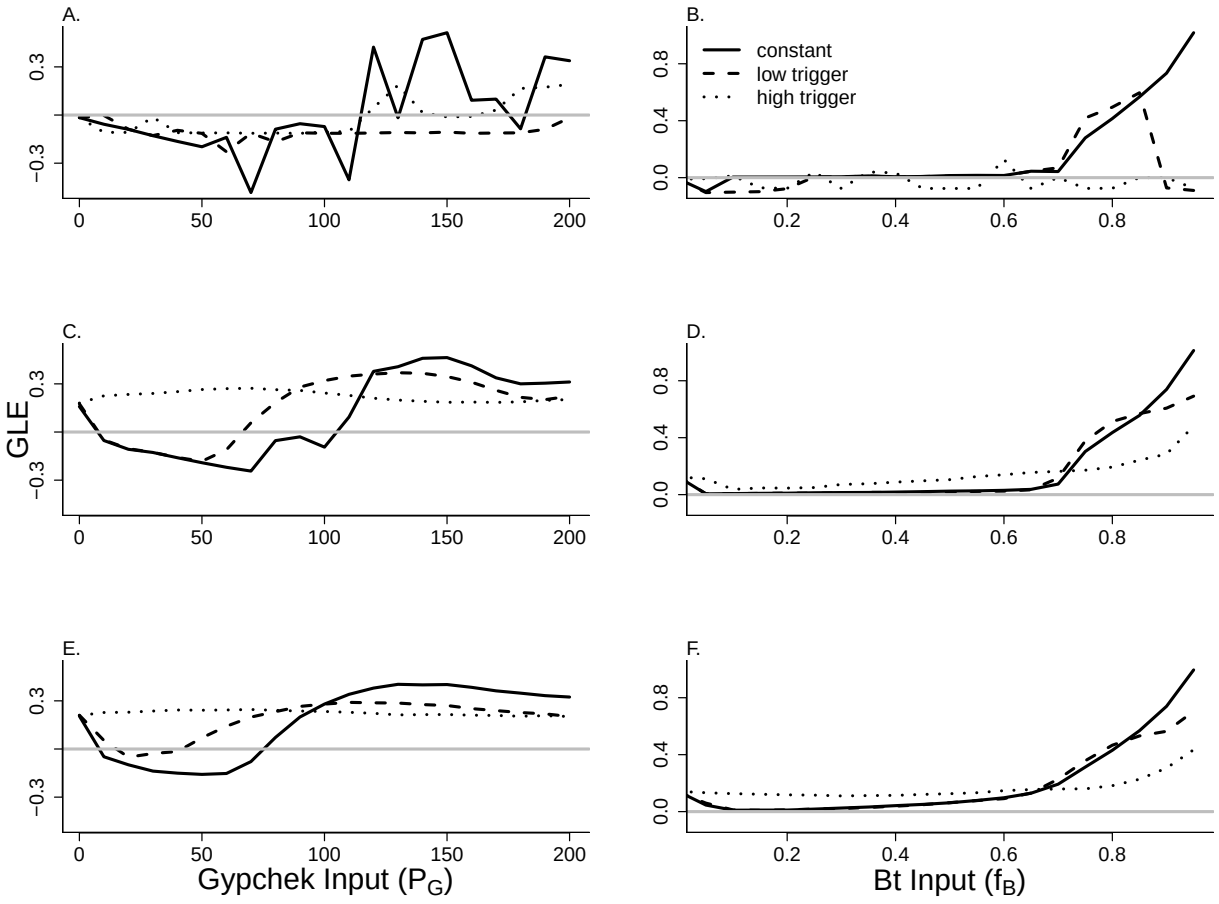

Figure S9: Effects of biocontrol input (P_G or f_B), threshold population size at which the biocontrol agent is administered (N_H), and stochasticity (σ) on the Global Lyapunov Exponents (GLEs) using the burnout approximation (eq. 3). The plots correspond to either Gypchek (A, C, or E) or Bt (B, D, or F) input with varying levels of stochasticity. For A and B, $\sigma = 0$. For C and D, $\sigma = 0.05$ and, for E and F, $\sigma = 0.15$. Three threshold triggers are plotted in each of the graphs corresponding to constant addition to the system (solid black line), a relatively low threshold population size of 1 (dashed black line), and a relatively high threshold population size of 10 (dotted black line). The gray line marks the division between chaotic (GLE > 0) and non-chaotic (GLE < 0) dynamics. Note the difference in GLE scales for Gypchek and Bt input.

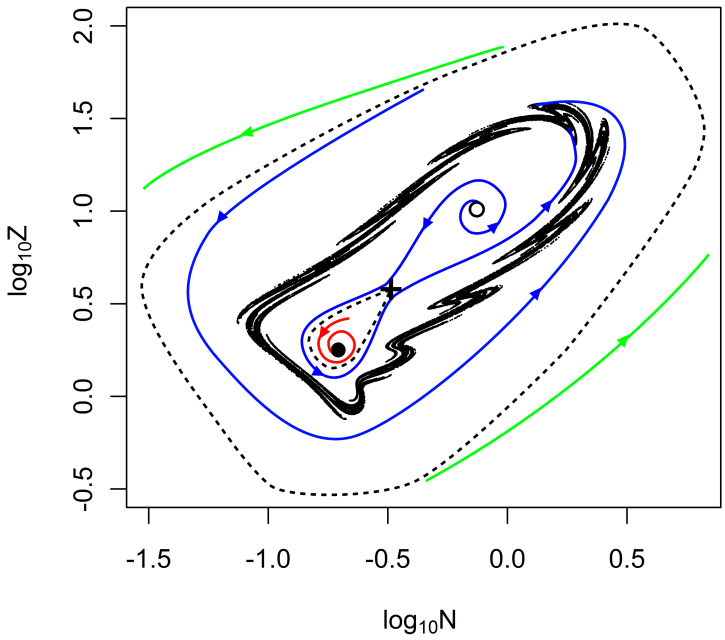

Figure S10: Plot of long-term dynamics of the basic model. The stable equilibrium (spiral) is a filled circle, the unstable equilibrium (spiral) is an open circle, the unstable saddle is a cross, and strange attractor (chaotic multi-year cycle) is plotted as an irregular black cloud of points (representing 100,000 generations on the attractor) that encircles the equilibria and the saddle. Locations of all phenomena were determined numerically. Illustrative trajectories are drawn to show system behavior in each region. The red arrow shows the path of trajectories converging on the stable equilibrium, the blue lines show trajectories entering the cyclic strange attractor, and the green lines indicate trajectories spiraling out to extinction. The outer dashed line represents the basin of attraction for the system. The inner dashed line is the basin for the stable equilibrium. Note the model dynamics are derived from the delay-differential equation model, eqs. S9-S19.

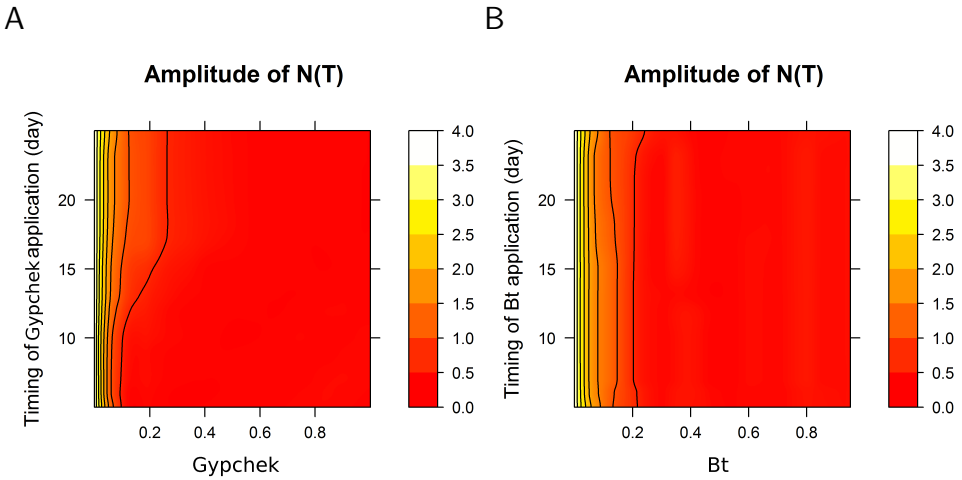

Figure S11: Plots of cycle amplitude values from the deterministic model for a range of within-season spray times and (A) P_G or (B) f_B values. All plots include only the 150 years following the start of the spray program. For these plots, $N_H = 0.25$. Note the model results are derived from the delay-differential equation model, eqs. S9-S19.

Supporting References

Abbott, K.C. & Dwyer, G. (2007) Food limitation and insect outbreaks: Complex dynamics in plant-herbivore models. *Journal of Animal Ecology*, **76**, 1004–1014.

Dennis, B., Desharnais, R.A., Cushing, J.M., Henson, S.M. & Costantino, R.F. (2001) Estimating chaos and complex dynamics in an insect population. *Ecological Monographs*, **71**, 277–303.

Dwyer, G., J. Dushoff, J. S. Elkinton, & S. A. Levin. (2000) Pathogen-driven outbreaks in forest defoliators revisited: Building models from experimental data. *American Naturalist*, **156**,105–120.

Dwyer, G., J. Dushoff, & S. H. Yee. (2004) The combined effects of pathogens and predators on insect outbreaks. *Nature*, **430**, 341–345.

May, R.M. (1974) Stability and complexity in model ecosystems. Princeton University Press. Princeton.

Murray, K. D. & J. S. Elkinton. (1989) Environmental contamination of egg masses as a major component of transgenerational transmission of gypsy-moth nuclear polyhedrosis-virus (LdMNPV). *Journal of Invertebrate Pathology*, **53**, 324–334.

Murray, K. D. & J. S. Elkinton. (1990) Transmission of nuclear polyhedrosis-virus to gypsy-moth (Lepidoptera, Lymantriidae) eggs via contaminated substrates. *Environmental Entomology*, **19**, 662–665.